UNIVERSIDAD COMPLUTENSE DE MADRID

FACULTAD DE CIENCIAS FÍSICAS

Máster en Astrofísica

TRABAJO DE FIN DE MÁSTER

En el abismo ultravioleta: explorando la destrucción estelar alrededor de agujeros negros supermasivos

Into the UV Abyss: Exploring Stellar Destruction Around Supermassive Black Holes

Julien Valteau

Supervisado por:

Erwan Quintin

Richard Saxton

Margherita Giustini

Curso académico 2025-26

Calificación: 9.7

Abstract - *Resumen*

The recent discovery of a years-lasting ultraviolet (UV) plateau following Tidal Disruption Events (TDEs, the destruction of a star by the tidal forces of a black hole at the center of a galaxy) opens a new window for their systematic study, with crucial implications for our understanding of supermassive black hole genesis. This long-lived emission signature enables retrospective searches through past UV survey data, offering access to a potential new population of TDE candidates.

In this work, we present an innovative multi-mission approach combining UV and optical photometric catalogs from the Ultra-violet Optical Telescope (UVOT) onboard the Neil Gehrels Swift Observatory (hereafter Swift), the Optical Monitor (OM) onboard XMM-Newton, and the Galaxy Evolution Explorer (GALEX), with over 12 million objects of all types. In an unprecedented approach, we systematically scanned the time-series light curves of the extragalactic subsample in search of TDE-like patterns in three UV bands simultaneously (UVW2, UVM2 and UVW1).

From this analysis, we finally selected 10 candidates that we consolidated using the available multi-wavelength information. However, given the serendipitous nature of the sources and the data quality limitations, these candidates should be regarded as promising rather than robust detections. Their confirmation will require the retrieval of mission raw data and, ideally, future UV satellite monitoring campaigns with renewed interest for this wavelength.

El descubrimiento reciente de mesetas ultravioletas (UV) durando anos después de los eventos de destrucción por marea (TDE, la destrucción de una estrella por la fuerza de marea debido a un agujero negro en el centro de una galaxia) abre una nueva ventana para su estudios sistemático, con implicaciones cruciales para nuestro entendimiento de la formación de los agujeros negros súper masivos. Esta emisión de larga duración permite buscar a posteriori en los datos archivados de las misiones UV, ofreciendo un acceso a toda una población de potenciales TDE.

En este trabajo, presentamos un nuevo método combinando los datos fotométricos UV y ópticos de los catálogos obtenidos desde UVOT (Ultra-violet Optical Telescope) a bordo del Neil Gehrels Swift Observatory, OM (Optical Monitor) a bordo de XMM-Newton y de GALEX (Galaxy Evolution Explorer), para un total de mas de 12 millones de objetos de todo tipo. De forma sin precedente, hemos recorrido sistemáticamente todas las curvas de flujo según el tiempo de los objetos extragalácticos, buscando los patrones fotométricos característicos de los TDE usando simultáneamente las 3 bandas UV (UVW2, UVM2 y UVW1).

De este análisis, hemos seleccionado 10 candidatos TDE que consolidamos usando la información disponible en otras longitudes de onda. Sin embargo, visto el carácter fortuito de las fuentes analizadas y los limitaciones de calidad de los datos, estos candidatos tienen que ser considerados como prometedores en vez de detecciones robustas. Su confirmación necesitara recuperar los datos brutos de cada misión y, idealmente, campanas de estudio de futuros satélites en UV con un intereso renovado por esta banda.

1 Context

1.1 Physical context

In recent years, the interest for stars destructed by Supermassive Black Holes (SMBH) has increased, as it constitutes one of the best probes to obtain information about the lower-mass SMBH, where direct dynamical measurement is not possible (Gezari, 2021). This information could help understand the demographics, the physics, and then the genesis of such SMBH. Today it is still not clear how the SMBH formed in a first place. One black hole seed formation model explains

growth through repeated mergers of smaller black holes (hierarchical model), so that getting this rate would provide information about the black hole occupation fraction in low-mass galaxies and then the probability of merging.

The theoretical concept of stars disrupted by SMBH through the tidal effect was first established in the late 1970s. A star is disrupted, once the tidal forces of the SMBH exceed the self-gravity of the star as described by the equation 1, where $R_\star$ and $M_\star$ are respectively the radius and the mass of the star, r its current distance from the black hole and $M_\bullet$ the mass of the black hole.

$$\frac{GM_\bullet R_\star}{r^3} > \frac{GM_\star}{R_\star^2} \tag{1}$$

Then the radius at which the disruption occurs, called the tidal radius, R_T will be:

$$R_T = R_\star(\frac{M_\bullet}{M_\star})^{1/3} \tag{2}$$

A fraction of the stellar material will be on unbound orbits and escape, while the rest will fall back towards the SMBH and eventually be accreted (Rees, 1988) as illustrate the Figure 1.

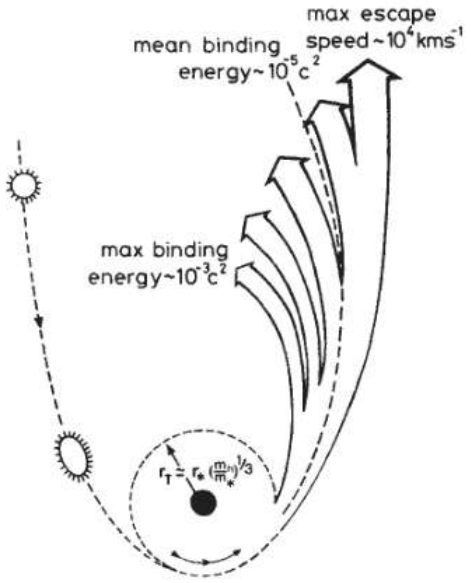

Figure 1: Schema of solar-type TDE with parabolic approach from Rees, 1988

These tidal disruption events (TDEs) result in luminous flares that in the last two decades have been observed across a wide range of observing frequencies, including hard X-rays, soft X-rays, optical and ultraviolet, infrared and radio. These emissions, that are still uncertain theoretically, primarily because of uncertainties in how the highly elliptical stellar debris stream circularizes, rapidly decreases as $t^{5/3}$ as shown in Figure 2, making the TDE hard to detect only weeks after the event. However, van Velzen, 2019 shows that late UV emission plateaus are still visible months or years after the event and have been interpreted as a signature of the emergence of the canonical accretion disk predicted by theoretical models or most recently viscously spreading accretion disk (Winter-Granic and Quataert, 2025). This long-lasting emission could allow us to go back in past UV observations and try to find yet undetected TDE plateaus. This is the goal of the work described in this document.

This work is exploratory, as systematic searches for UV plateaus have, to the best of our knowledge, never been done before, using a multi-mission approach. It is an opportune moment to

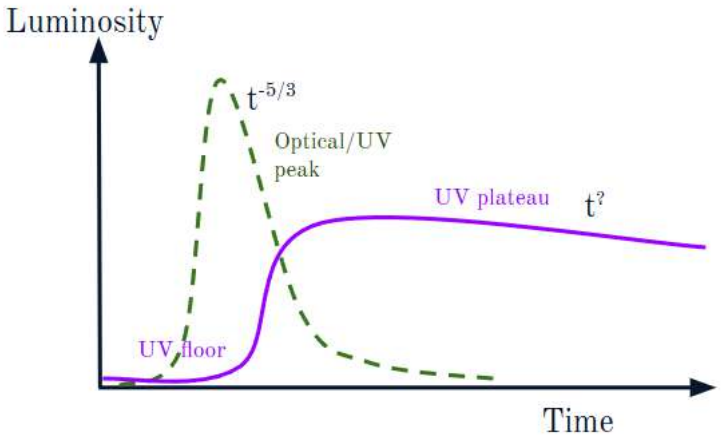

Figure 2: Schema of TDE expected flux evolution in optical and UV band

perform it, as Swift will be back to be available soon and a new ultraviolet mission that will study TDE is planned to be launched in 2027 (Ultraviolet Transient Astronomy Satellite, ULTRASAT).

1.2 Data context

In order to find TDE signatures, available UV catalogs will be used instead of raw mission data. The main purpose of using catalogs is that they have been cleaned from most of the defects affecting the raw data observations (e.g. instrument sensibility changing according the time) and it is considerably smaller in terms of storage, containing the minimum required for our investigation (flux at a specific date for a given source). We will look for serendipitous UV plateaus, i.e. sources that were not the target of their observation but simply were present, by chance, in the field of view at the right moment. As this is unlikely, to maximize our chances we compile together data from various missions. The UV databases used in this work are coming from GALEX, XMM-Newton and Swift observations. The three missions had different objectives and very different designs that are important to understand before merging them into a single UV catalog.

1.2.1 GALEX data

GALEX was a National Aeronautics and Space Administration (NASA) space telescope that has been active from 2003 to 2012 and thanks to its Field of View (FoV) of around 1.2° conducted an all-sky survey in two bands: Near Ultraviolet (NUV) from 1771 to 2831Å and in Far Ultraviolet (FUV) from 1344-1786Å. It was the first sky-wide UV survey. The GALEX UV catalog used corresponds to the data release 6-7 (GR6plus7) and is the last available (Bianchi et al., 2017). It provides us a single detection per source. The duplicated detections of a source have been removed, selecting the one with the larger exposure time or, if exposure times are the same, the one where the source is the closest from the field center. Due to this specificity, the date of each detection is not directly available in the catalog which is a problem for this study that aims to get time series detection. A solution to obtain the detection dates is described in section 2.2.4. Other criteria are used to select the sources in the catalog:

- Only sources that are closer than 0.55° from the field center, to avoid sources with poor photometry and astrometry near the edge of the field, and rim artifacts.
- Only sources with NUV magnitude error inferior to 0.5mag. This is almost all NUV detection. Sources with FUV detection and no NUV detection are very rare and will not be in the catalog.

For information, around 10% of NUV detection have a FUV counterpart.

- Only sources where both NUV and FUV detectors were turned on. This criterium ensures that source non-detection in FUV corresponds to sources that are too faint to be detected and not to observations with the FUV detector turned off.

Finally, the catalog contains 82,992,086 sources for a covered area of 24790 deg^2 (around 60% of the sky). It has been downloaded in this study from http://dolomiti.pha.jhu.edu/uvsky/GUVcat/GUVcat_AIS.html where it is available in slices of 5° of galactic latitude. Note that the coverage around the galactic center is lower due to the thin disk galactic dust extinction as it can be seen in Figure 3. As it is less sensitive than the other telescopes (typical depth of 20.8 mag in NUV and 19.9 mag in FUV for a normal exposure of 100s for the all sky survey) but covered a large part of the sky, the GALEX catalog could also be us to get upper limit for faint sources that have not been detected but which area has been covered by GALEX. For this work, an internal ESA tool computing GALEX upper limit will be used.

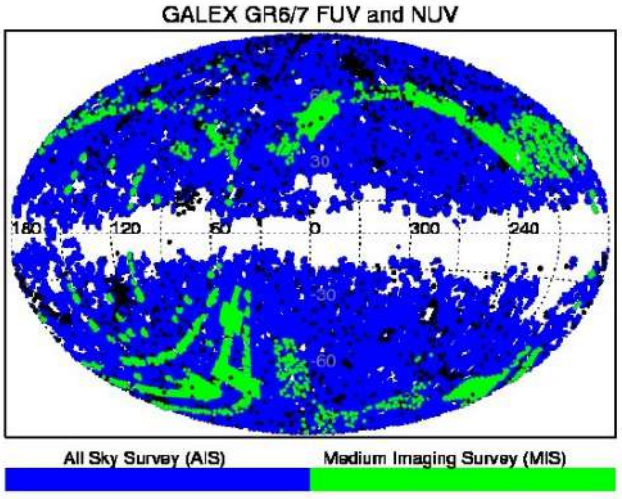

Figure 3: GALEX coverage sky map with FUV an NUV detectors on from Bianchi et al., 2017

1.2.2 XMM-Newton OM data

XMM-Newton is a European Space Agency (ESA) satellite that is active since 1999. Its design has been mainly driven by the objectives of X-ray investigation. The main rational of its ultraviolet and optical instrument, the Optical Monitor (OM), is to provide complementary data to those from X-ray instruments, in particular to create a simultaneous multi-wavelength capability to constrain spectral energy distributions, as explained Page et al. (2012). Its eccentric orbit (e=0.81) allows to get large continuous exposure time (until 2 days) which leads to low error on flux measure. Its FoV is around 17x17 $arcmin^2$. For UV data, both characteristics (FoV smaller than GALEX and large exposure time) imply a small amount of sources covered with excellent quality. Apart from the 3 optical bands (U, V, B), OM operates in 3 UV bands (from the most to the least energetic) : UVW2 (λ_{eff} = 2120 Å), UVM2 (λ_{eff} = 2310 Å) and UVW1 (λ_{eff} = 2910 Å) with a magnitude distribution peak of respectively 20.2, 20.9 and 21.2 mag.

Its catalog contains all available detections for each source, so that single sources could have multiple detections. In total, the XMM-Newton Serendipitous Ultraviolet Source Survey (XMM-SUSS) catalog from OM data in its version 6 used for this study contains 9,920,390 detections made between 2000 and 2022 for 6,659,554 sources. It is available for download at the following

link: https://nxsa.esac.esa.int/catalogues/XMM-OM-SUSS6.2.fits.tar.gz. The UVM2 band is the closest to the GALEX NUV band as can be seen in Figure 4 which compares both satellite bands.

Two important additional flags are provided for each band in the catalog:

- One related to the extension of the source. If the source is extended, the flag is set to true. It is a conservative flag, which means that in case of doubt regarding the resolution of the extended source, it will be considered not extended by default.
- Another one related to the quality of the detection. This flag is set to a value different to zero in case a type of defect can be observed for this detection.

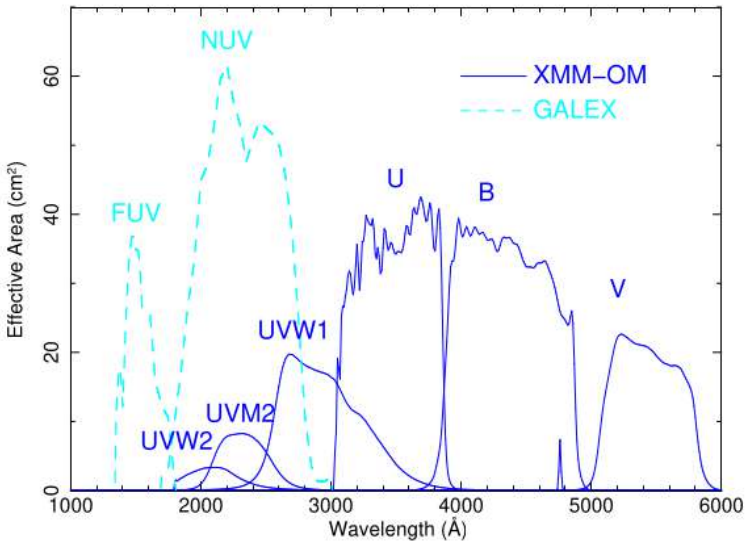

Figure 4: Comparative of the GALEX and OM bands from Page et al., 2012

1.2.3 Swift UVOT data

Swift is a NASA satellite active since 2004. As XMM-Newton, ultraviolet observations are complementary to the gamma and X-ray data collected in the frame of its main investigation, observing gamma-ray bursts (GRB) and its afterglow. The design of its Ultraviolet/Optical Telescope (UVOT) is very similar to XMM-OM, on which it is based. However, its Low Earth Orbit (LEO) leads to very different set of data with a lot of short exposure observations (maximum 1h), leading to higher flux error. Its FoV is around 17x17 $arcmin^2$, as XMM-OM, and uses also the six same bands UVW2, UVM2, UVW1, U, V, B.

The catalog used contains a total 13,860,569 detections for 6,200,016 sources for an observation period from 2005 to 2010 (Page et al., 2015). It is available for download at the following page: https://www.mssl.ucl.ac.uk/www_astro/uvot/uvotssc/. The catalog contains also quality flags and extension flags associated to each detection.

1.2.4 Catalogs timeline summary

A summary of the timeline of each catalog used in this study is presented in the Figure 5.

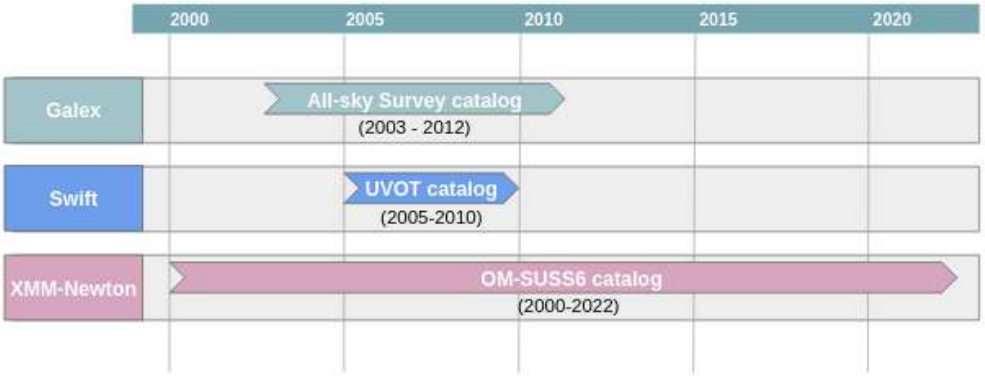

Figure 5: Catalogs timeline summary

2 Methods

All scripts described in this section have been saved in the following Git repository https://github.com/JulienValteau/TFM_TDE_Detection/tree/main/UV_database_creation_pipeline

2.1 General combined UV catalog creation

The creation of the combined UV catalog, aggregating the databases from the various telescopes mentioned, required various process steps. This creation pipeline is represented in Figure 6. In the frame of this work, as TDE identification requires various detection along the timeline, only UVOT and OM are fully combined. GALEX catalog which provides a unique detection by source is used to complete the detection set associated to sources in UVOT or OM. Doing so allows to avoid using a lot of memory for GALEX sources with only one detection and no counterpart in UVOT or OM. This could be a limitation for others UV data exploration works that should be taken into account.

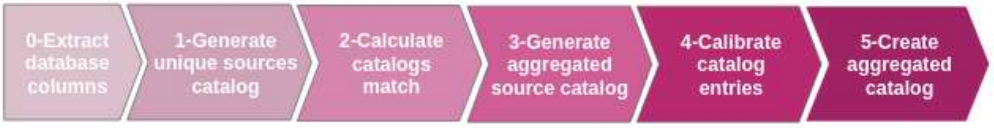

Figure 6: Combined UV catalog creation pipeline

The steps 0 and 2 are bash scripts calling the powerful STILTS tool that allows to perform operations on very large table dataset. Its documentation can be found on the following page https://www.star.bristol.ac.uk/mbt/stilts/. The rest of the scripts are written in Jupyter Notebook format.

2.1.1 Extract database columns

This first step is necessary considering that:

- The complete databases occupied a lot of memory (around 5 Gb for UVOT and OM databases and 18 Gb for the compressed GALEX database).
- All necessary data are not in the same data table from the Flexible Image Transport System (FITS) file. In particular the time of the detections for UVOT and OM are in the observations table instead of the detection table.

Thus, during this step, only the mandatory columns are extracted: Observation identifier, source number, coordinates, positional error, flux values in each band and its associated flux error, quality flag and source extension flag. The detection time is obtained by matching the observation number within the observation table. As the data are huge, the match is performed slicing the observation table into smaller parts. Then the slices with all the columns are concatenated and the results are saved in two tables in order to get smaller resulting tables: one with all sources information (source number, coordinates and positional error) and the other with all specific detections information (source number, flux and its related columns and observation dates).

Note that for UVOT two specific transformations of the initial database columns are necessary. First the positional error (δ_{POS}) is given as right ascension error (δ_{RA}) and declination error (δ_{DEC}). The error is defined according to the documentation as σ distribution error. Those columns are combined to get a unique positional error using the formula 3:

$$\delta_{POS} = \sqrt{(\delta_{RA} \cdot \cos(DEC))^2 + (\delta_{DEC})^2} \tag{3}$$

Then the time has to be converted from ISO8601 (e.g. 1994-12-21T14:18:23.2) to Modified Julian Date (MJD). This function is directly available in STILTS as isoToMjd() function.

2.1.2 Group detections by source

For each detection in UVOT or OM catalog is given the estimated position in right ascension (RA) and declination (DEC) of the associated source, which is slightly different in each case even if the source is the same. Before performing a cross-catalog match of the sources catalog, a single weighted average position of the sources per catalog is calculated using a weighted average:

$$RA = \frac{\sum_i RA_i/\delta_{RA_i}}{\sum_i 1/\delta_{RA_i}} \qquad DEC = \frac{\sum_i DEC_i/\delta_{DEC_i}}{\sum_i 1/\delta_{DEC_i}} \tag{4}$$

To perform this operation correctly and avoid coordinate singularities at the poles, the RA near 360° are shifted near 0° if the standard deviation of the RA associated to a source is detected to be higher than an arbitrary threshold. Then the weighted average RA calculation is performed and the result is moved back near 360° if the resulting value is negative. A sanity check is performed to check that no negative RA remains at the end of the treatment. In addition, various calculations are drawn to visually check that the shape is as expected, with a weighted position within the area formed by the original position as in Figure 7.

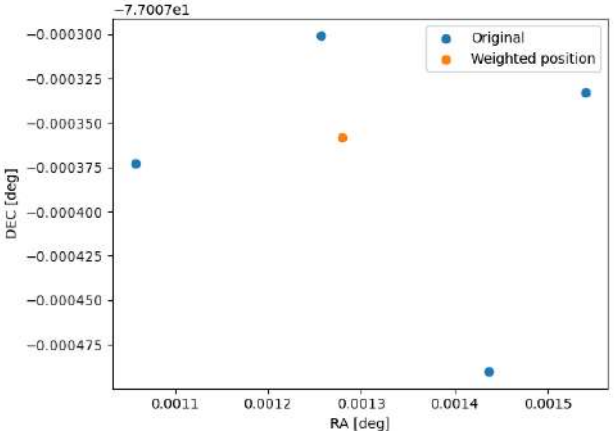

Figure 7: Example of results for weighted position calculation

Regarding the single positional error of a source, the mean of its errors of position is taken into account, in a conservative approach.

2.1.3 Cross-match

Once a unique position and error are defined for each source of each catalog, the next step is to perform the cross-match of each catalog to cross the detection information. To do so, scripts in STILTS are used calling the tmatch2 function that implements k-d tree algorithm. First proposed by Bentley, 1975, the main principle of this algorithm is to partition one of the catalog to match into a binary tree, splitting step by step each cell by its median point until only one point remains in each cell. This tree shape partition allows to reduce the complexity of the matching from $O(n^2)$ for the naive approach to $O(nlog(n))$, which is important for our catalogs with millions of entries.

For this specific work, the matching algorithm used through STILTS is set to:

- Take into account a tolerance of 3σ on the position error of both catalogs.
- Return only the best match and not all matches possible.
- Find matches for all sources in both catalogs.

The result in terms of angular distances of the matching sources is expected to be the shape of the convolution of a Rayleigh distribution related to the significant matches and a gaussian distribution corresponding to the random matches related to the sources density. Even if they are independent, two populations of sources in the sky have, indeed, a non-zero fraction of matching points, due to the presence of positional errors. These are called "random matches", and can lead to spurious associations of independent physical objects. The impact of these random matches is evaluated by performing multiple matches shifting one catalog from 1 arcmin in various directions. Doing so allows to create random catalogs with a shape that reproduce the geometric structure of the real catalog in terms of sources density distribution according the coordinates.

The first cross-match to be performed is between OM and UVOT catalogs. Before looking at the results in terms of angular distances, the results are drawn with respect to the two directions (RA, DEC) to determine if any constant bias or anisotropy exists. In Figure 8a it can be seen that the deviation distribution is approximately circular and the systematic error is low (around 0.13 arcsec).

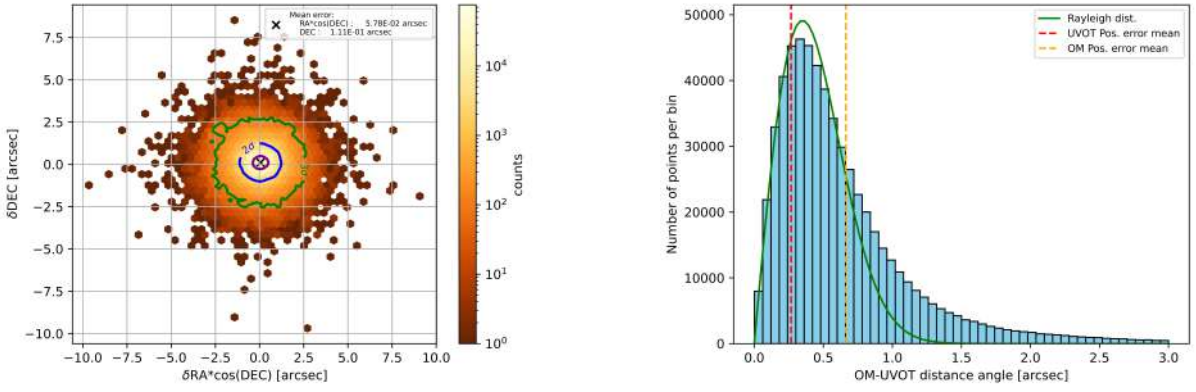

(a) Coordinates deviation

(b) Angular distance distribution

Figure 8: UVOT-OM matching sources distance distribution

We obtained 595,146 matches, which represent, respectively, 8.9% of OM sources and 9.6% of UVOT sources. This number is on the order of magnitude of the expectation, considering the very

different objectives of the XMM-Newton and Swift satellites. The angular distance distribution of the matches is as expected coherent with a Rayleigh distribution, as can be seen in Figure 8b.

The random matches check provides a mean of around 104,000 matches, so that we can expect that a number around this value within our matches is due to random matches. Considering that random matches are more likely to occur for the highest angular distance, we can estimate the angular distance at which 104,000 matches from our matches have a higher angular distance. This corresponds to around 1 arcsec. In order not to be too restrictive, a cut-off value of 1.5 arcsec is defined. For higher angular distances, sources from both catalogs are considered different.

As TDEs are extragalactic events, and to reduce the size of the data early in the process, the OM and UVOT catalogs are matched with the most complete galaxy catalog, Regalade (Tranin et al., 2026) which merges various existing galaxy catalogs. This is a limitation of the combined UV catalog in the frame of future works with different objectives. The same approach is used to check that the match is performed correctly and to select the cut-off value. The angular distance distribution resulting from those catalogs matches is presented in Figure A.1. Shapes are following Rayleigh distribution as expected and the cut-off value of 1.5 arcsec is defined leading to select 305,209 sources for OM and 280,270 sources for UVOT from which 21,138 are in both catalogs.

At this step, the sources are combined into a single source catalog. To do so, a single weighted average position of the sources is calculated following the formula in section 2.1.2.

Once the UVOT-OM combined source catalog is created, the match with the GALEX catalog is performed. As GALEX position error and Full Width at Half Maximum (FWHM) are higher than for UVOT and OM, the matches are more suspicious. For this reason, a flag is added in the database to define suspicious matches where the associated source has various possible matches. These sources are obtained comparing the resulting matches using "all matches" option and "best only" option. Additionally, to better take into account an instrumental systematic error, in particular for the brightest sources where the positional error is supposed to be lower, the matches are made considering the maximum of the 3-σ positional error associated to this source and 3 times the positional error mean of all sources. The number of matches obtained is 243,132 which corresponds to 43% of the combined UVOT-OM galaxy catalog. From this number of matches, 2,827 (1.1%) are considered suspicious. Three main reasons can justify why the number of matches with UVOT-OM catalog is not higher:

- The UVOT-OM source corresponds to an area that has not been visited by GALEX.
- The sources position computed for GALEX is too far away from the source position computed for UVOT and OM catalog.
- The source was too faint to be detected by GALEX. The corresponding upper limit could be additional information for TDE candidates, as the TDE implies a drastic increase of the UV band flux.

As in the previous match, the mean offset is low (around 0.11 arcsec) and the deviation distribution is approximately circular as it can be seen on Figure 9a. Figure 9b) shows that the shape follows a Rayleigh distribution. The cut-off value is defined using the mean random matches value around 13,600. In this case, a 4 arcsec cut-off value is selected which leads to keep 232,506 matches from which 2,574 are still suspicious. These data are added to the combined catalog using a default date corresponding to the latest date possible for GALEX (2012) as the real date is not available. The real date will be obtained doing a workaround with the internal ESA tool used to get GALEX upper limit for source candidate only and is described in section 2.2.4.

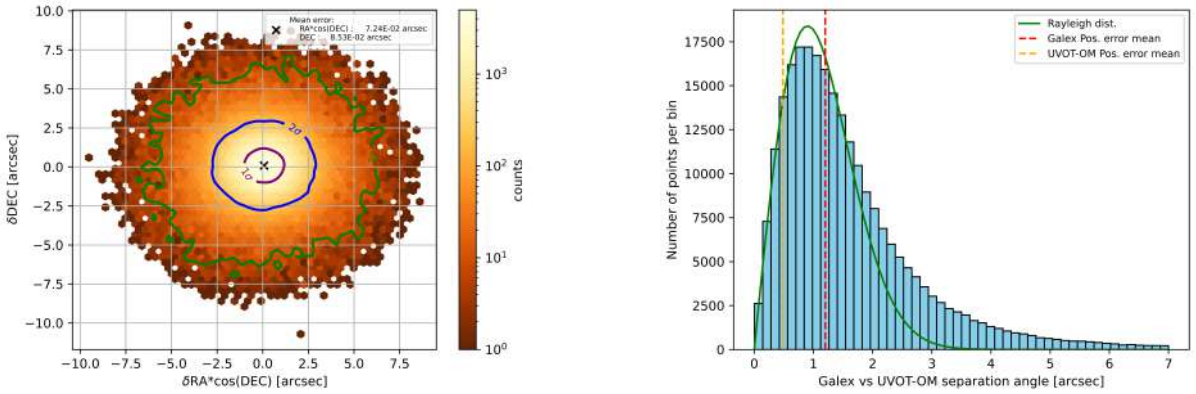

(a) Coordinates deviation

(b) Angular distance distribution

Figure 9: GALEX vs UVOT-OM matching sources distances distribution

2.1.4 Calibration

Once the matching of all sources cross-catalog is performed, it is possible to calibrate the measured flux cross-instrument. This step is crucial for our study that aims to detect flux variations along the time by combining all instrument information. If the match of the sources information within each catalog and cross-catalog is correct, the fluctuations of a source can have 3 origins:

- The statistical measurement error itself, which leads to get different measurements each time.
- The calibration between the instruments, which leads to get different measurements according to the instrument used.
- The physical variation of the source itself which is what we want to isolate for this work.

Before performing the calibration between the instruments, the shape of measurement spread of each instrument is obtained by crossing together all measurements per source by a single instrument. Note that for this analysis, only the galaxy source measurements with no known defects (quality flag at 0) are used.

As expected the shape is symmetrical around the diagonal with higher spread on the faintest sources and lower on the brightest as it can be seen on an example for UVW2 on Figures 10a and 10b. The spread is also higher for UVOT than OM with at max a flux spread factor of around $10^{1.5}$ versus 10 for OM which is also expected considering the lower exposure times and hence larger measurement errors available on Swift. Lastly it can be observed that for the brightest sources the spread increases for UVOT. This can be explained by the nature of the Swift mission, mostly aimed at monitoring variable bright sources.

At this step, the calibration between OM and UVOT flux can be performed. The aim of this operation is to get comparable flux on average between instruments for a given source. Even if the absolute value is not critical for our study, as the TDE detection implies to look for relative flux variation, it is decided to use OM flux as a reference and correct UVOT values, as OM flux errors are generally lower. A 3 order polynomial fit is used to perform the calibration, taking into account the error through the Python ODRpack library (weighted orthogonal distance regression solver available at https://pypi.org/project/odrpack/) which takes into account the error of the variables to perform the regression. The results are quite similar to a simple polyfit solution from the Numpy package, only on the flux range boundaries changes are noticeable. Tests with spline functions have

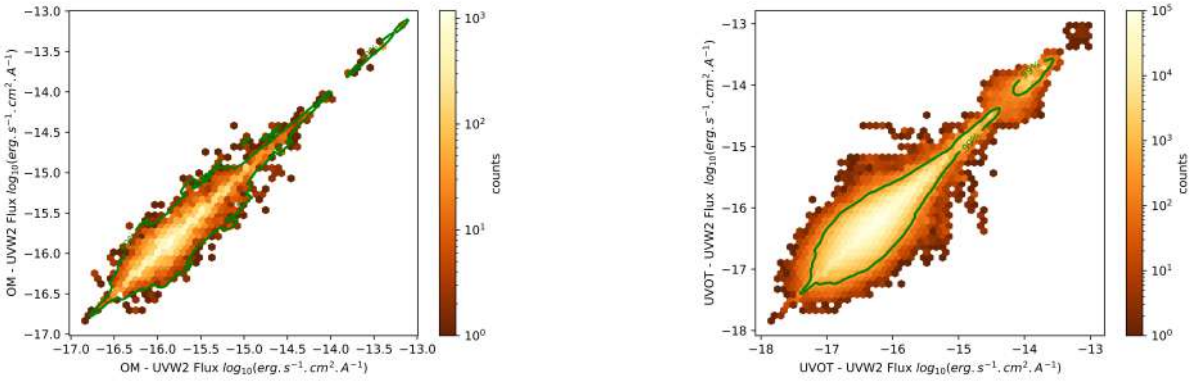

(a) OM versus OM

(b) UVOT versus UVOT

Figure 10: Cross-measurements per source for UVW2 band - Green contour represents 99% of the data distribution

been performed, but are not adapted to our problem where a distribution is considered. Spline are more adapted to signal changing over time for example. An example of calibration curve and residuals $((flux_{UVOTcalib} - flux_{OM})/flux\ error)$ for UVW2 is presented on Figure 11.

For more precise results and as the extended flag is available for both catalogs, two calibrations are performed: one for the extended sources (left) and one for the not extended sources (right). As extension flag is computed according count extension and could be different in both catalogs, if any catalog computes that the source is not extended, the source is considered as not extended to be conservative.

The final shape of the residuals is around $\pm 12\sigma$ for all bands for 95% of the distribution for extended sources and $\pm 11\sigma$ for not extended sources. An outlier is visible on the residuals on the brightest side for the UVW2 band. This corresponds to a unique source that has been seen repeatedly (59 times) by UVOT. This repetition artificially increases the population of entries for the brightest sources where the polynomial fit is the worst. Also the image identified 506200201 in the OM catalog has been removed, as an unexpected defect (flare on the edge) is making the indicated flux incoherent for all sources in the image.

The same approach is used for GALEX with respect to OM entries, calibrating the NUV and FUV bands with respect to the 3 OM UV band (UVW2, UVM2, UVW1), except that a unique calibration is performed as no extended flag is available for GALEX. An example of the calibration and residuals obtained for NUV with respect to UVW2 are presented in Figure A.2. Note that this calibration includes the conversion from Jy to $\mathrm{erg\,s^{-1}\,cm^2\,A^{-1}}$.

The shape of the residuals is also as expected with residuals higher for the brightest source, where the flux error is lower. For NUV band, the residuals are around $\pm 10\sigma$ with respect to UVW1, UVM2 and UVW2 for 95% of the distribution. For FUV band, the residuals are slightly lower around $\pm 7\sigma$ for 95% of the distribution. This lower sigma can be explained by the higher FUV flux error.

For the error, the calibration is performed following the formula 5 that considers a first order approximation which is acceptable for our work.

$$flux\ error(x)_{cal} = flux_{cal}(x + error) - flux_{cal}(x) \tag{5}$$

The calibration resulting polynomial coefficients are presented in Table B.1. Note that even if a third order fit regression is used, almost no calibration required a coefficient for the last order. So that a second order fit regression appears to be enough.

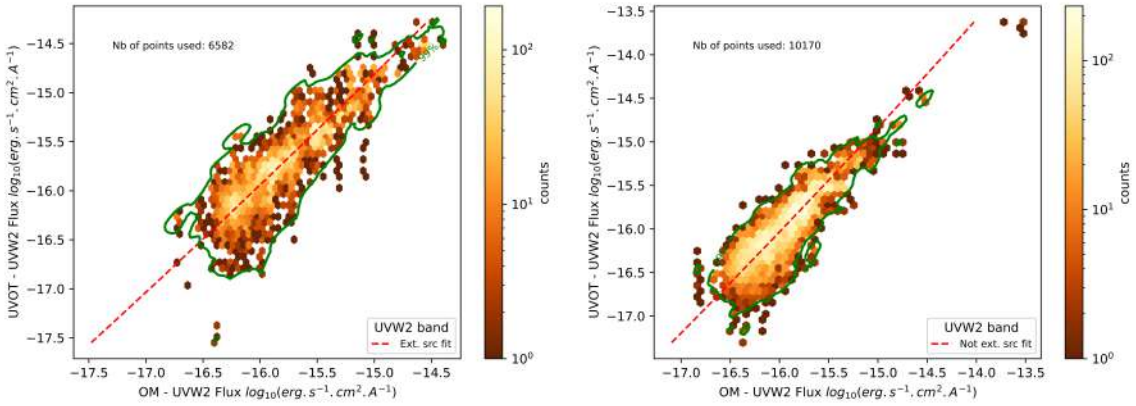

(a) UVOT vs OM flux per source - Green contour represents 99% of the data distribution

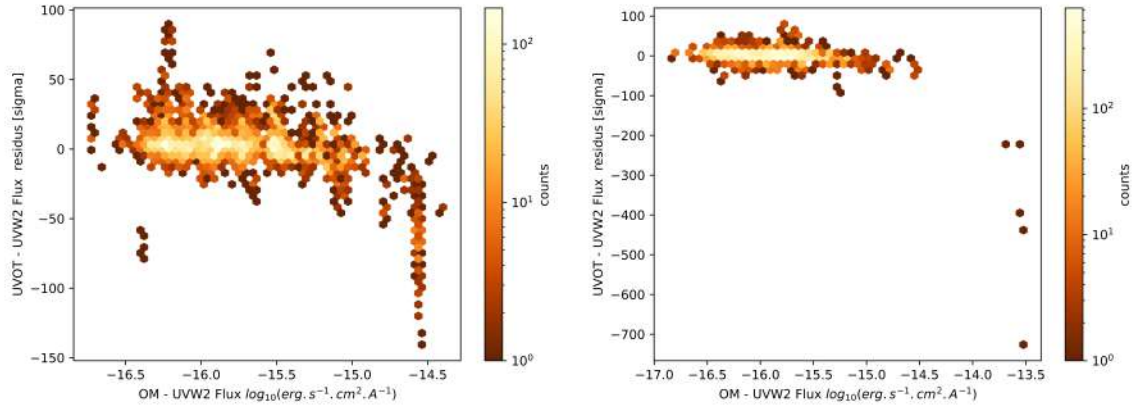

(b) UVOT residuals versus OM flux

Figure 11: UVOT calibration with respect to OM for UVW2 band (extended on the left, not extended on the right)

Once calibrated, all catalogs can be merged in a unique combined ultraviolet catalog. Note that for the GALEX catalog, since the date of the detection is not known, by default a date corresponding to the latest possible date is inserted (2012). Doing so allows to use the measurements in this catalog when looking for UV plateau to get an approximate light curve shape.

2.2 Candidates selection

All candidates selection and analysis have been performed using Python and a few Jupyter Notebooks. All corresponding scripts are available at https://github.com/JulienValteau/TFM_TDE_Detection/tree/main/TDE_filtering_and_analisis. Most of the filtering and analysis use Pandas Dataframe library, in particular the groupby methods with aggregating built-in functions (sum, mean, count, etc.) for more efficiency. The solution using SQL queries building a combined ultraviolet catalog as a relational database has been studied but not retained. This alternative is inefficient with respect to loading the data in the memory as a dataframe since the catalog size has been reduced drastically when filtering only galaxy objects (3.2 Gb to 300 Mb).

2.2.1 Known TDE analysis

In order to understand how to detect the potential TDE candidates within the combined UV catalog, a primary analysis consists in looking at a catalog of known TDEs and see their light-curve's shape within our data. For this exercise, we use the most complete TDE catalog available, constantly updated, the OTTER (Open mulTiwavelength Transient Event Repository) catalog available at https://otter.idies.jhu.edu/. When matching it with our catalog, only 20 TDEs have ultraviolet or optical data from the 239 available. Of these 20 TDEs, only 7 have more than 3 points necessary to appreciate a shape and only 3 from these 7 have enough time range to include an interesting part of the TDE. The two best examples are presented in figure 12. Hereafter are the characteristics we can observed using our catalog data on these 3 TDE.

- **2018fyk** has a GALEX point before the TDE and OM points after, so that the flux jump can be appreciated from 3×10^{-17} to 3×10^{-16} erg s^{-1} cm^2 A^{-1} in the UVW1 band. The flux is multiplied by 10 after the TDE.

- **Dougie** is observed by UVOT during around 30 days after the TDE which allows to appreciate the light curve fast decay part. As the decay in UVW1 goes from $2 \times 10^{-15} \pm 0.1$ to $2.5 \times 10^{-17} \pm 0.1$ erg s^{-1} cm^2 A^{-1} in 30 ± 0.1 days ($0.08 \pm 3 \times 10^{-3}$ years), we obtain an exponent of -1.73 ± 0.1 which is compatible with -5/3 law (-1.66). But unfortunately, no plateau is visible, which is what we expect to filter for this work, as it is very unlikely to catch a TDE in the 30 days after the event with enough detection points to obtain this fast decay shape.

- **ASASSN-14li** allows to appreciate a jump (from 4×10^{-16} to 7.5×10^{-16} erg s^{-1} cm^2 A^{-1} between both plateaus) and an ultraviolet plateau (UVW1) during around 1500 days (4 years) thanks to UVOT observation. During those 4 years the ultraviolet seems to slowly decay from 7.5^{-16} to 6×10^{-16} erg s^{-1} cm^2 A^{-1}.

Considering this low number of known TDE in the data, the initial idea of using machine learning to detect TDE shape in the data is discarded. Instead, it is decided to analytically filter the data, searching for the flux jump between both plateaus, as described in the next section. Note that doing so, extracting the host galaxy emission part is not critical, as it is the differential flux evolution that is analyzed, assuming that all changes are due to the TDE and that the host galaxy emission part is not changing.

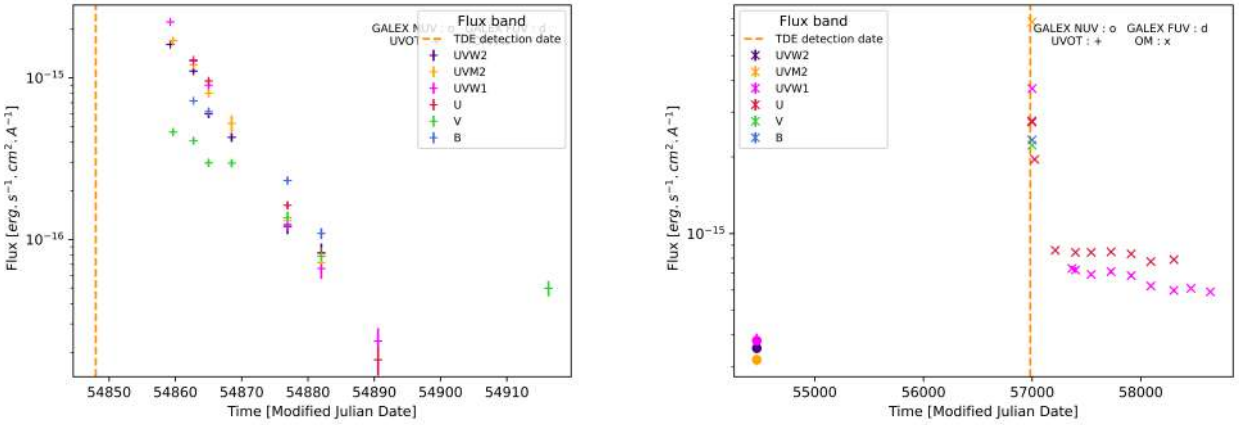

(a) Dougie (b) ASASSN-14li

Figure 12: Known TDE light curves with combined UV catalog

2.2.2 General candidates selection approach

Starting from the catalogue of extragalactic sources, we choose candidates from their light curves by:

1. Filtering for jump in mono-band or with a combination of bands information (UV color change).
2. Inspecting visually the mono-band light curves of the candidates to eliminate the ones that do not have the expected shape.
3. Generating the all-band light curves and visual inspection of them to eliminate those that do not have the expected shape.
4. Collecting complementary information (multi-wavelength, physical parameters in the literature for the associated sources, described in section 2.2.4).

As the filtering criteria are quite simple, hundreds of candidates are obtained in the first step and are necessary to inspect. Various situations could lead to exclude the source from the candidates:

- When having a negative peak, the variability is first negative then positive and could raise our threshold. These negative peaks are not the shape we are searching for and should be eliminated.
- If the jump occurs in the last measurement, it is impossible to observe any plateau. Even if the object could be a TDE, it is discarded as a candidate.
- If jumps from various sources are related to the same observation, the observation could be affected by a defect. This is how OM observation 506200201 has been detected to be erroneous.

2.2.3 Filters applied

Considering the emission variability from a detection to the next one, the jump from the UV floor to the UV plateau will correspond to a unique peak of variability. A first approach has been to compute the variability as a difference of flux from one detection to the next, and search for sources

that have a unique peak of variability in any ultraviolet band. As each measurement has its own error, the difference is normalized considering the error with the formula 6. The threshold used during this first analysis is a jump of 30σ, considering that 100σ is reached for ASASSN-14li (see Figure 13a).

$$diff = \frac{detection(x+1) - detection(x)}{\sqrt{error(x+1)^2 + error(x)^2}} \tag{6}$$

Even if a few objects have been retained for further analysis by this method, it shows a great limitation as the filter depends on the absolute flux.

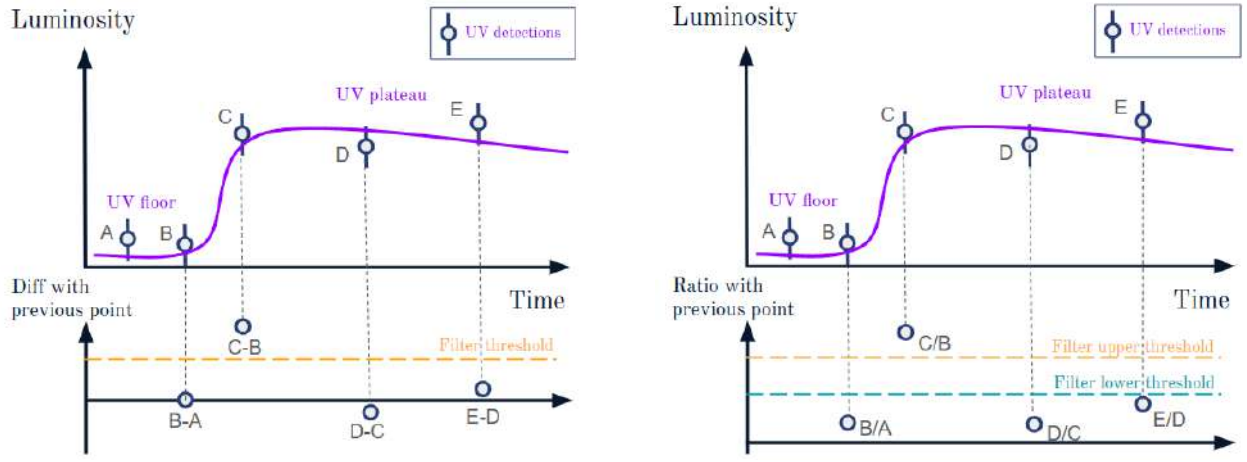

(a) Flux difference method

(b) Flux ratio method

Figure 13: Filtering methods schema

Another approach consists in looking at sources with a unique jump computed as a ratio of flux. For this method a second filter has been applied to ensure that the rest of the ratio remains within a threshold to be sure it is more or less constant (see Figure 13b). Various flux ratios have been considered for the jump: 5, 4 and then 3, each time searching for the new candidates only. The plateaus have been filtered considering only the ratio lower than 2 from one to another. Note that filtering for plateaus would require another lower threshold to eliminate the candidates where a peak down occurs (ratio inferior to 1). This additional filtering is performed manually during the visual inspection.

We think that TDE plateau emissions will be more likely in the most energetic UV band. For this reason, when using the lowest peak thresholds (4 and 3), we tried to detect candidates with peak of ratio variability in:

- UVW2 only with no change in UVM2 and UVW1
- UVW2 and UVM2 only and with no change in UVW1 band.

Also candidates where UVW1 has a ratio variability peak whereas the most energetic bands are not changing are not retained as TDE candidates. The method using a variability defined as a ratio, is the one that provided most of the candidates.

A last approach, presented in Figure 14, consists in looking for ultraviolet color changes. The idea is that if the less energetic bands emission are not affected by the TDE emission, whereas the more energetic bands flux are jumping for a plateau to another higher, the color in UV of the object (UVW2-UVW1, UVW2-UVM2, UVM2-UVW1) could be inverted. So the last filtering used select an object as a candidate if one of the listed ultraviolet color changes of sign. This approach leads

to few more candidates has the approach from the last section (ratio variability jump) includes sources with ultraviolet color changes.

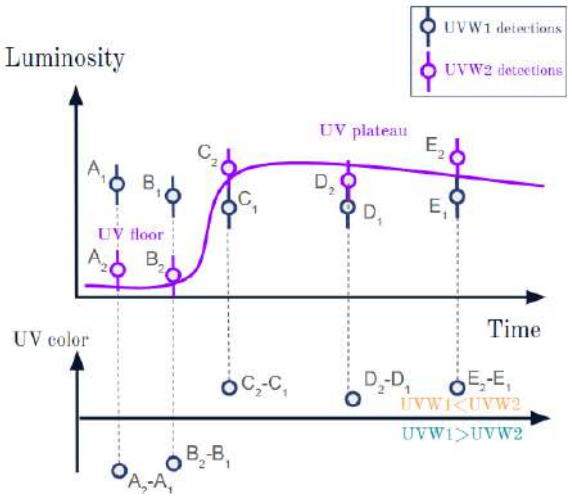

Figure 14: UV color filtering method schema

2.2.4 Additional analysis

Once a filtered source has been retained according to its visual inspection, various additional analysis are performed to consolidate it.

Firstly if the source has no GALEX detection associated, an internal ESA tool is ran to try to get its associated upper limit. This tool runs through the GALEX catalog and if no detection is found, runs through the observations coverage map. If the source area has been covered without detecting it, an upper limit can be added, estimated from the instrument's background value at this point in space and time. As the observation has an associated date, the upper limit can be dated and the point will be added on the light curve. On the other side, if a source has a GALEX detection, the same tool can be use to determine its exact date. To do so, 4 points forming a cross around the source are analyzed (first at 1 arcmin then at 20 arcsec, if the first try failed), searching for upper limit. If 3 points at least provide the same upper limit time, the source detection date is set to this upper limit time. Note that it is used at this stage and not to add date directly within the combined catalog because this tool is not designed for massive queries in a loop.

Secondly the information from the Regalade catalog is retrieved, in particular:

- The mass of the galaxy. If a jump in an energetic ultraviolet band occurs in a small galaxy, it is more likely to be due to a TDE, which prefer lower mass black holes. For large galaxies, with a large central SMBH, the tidal radius is below the event horizon, and thus the TDE happens in the black hole and is invisible.

- The difference between W1 and W2 Wide-field Infrared Survey Explorer (WISE) band according to the criteria defined by Stern et al., 2012. If the absolute difference is lower than 0.8 mag, the target is passive with a reliability of 90%.

Note that these data are not always available, as Regalade is a patchwork of galaxies catalog with various information coming from each catalog.

Thirdly, the appearance of the source is observed on ESAsky website (https://sky.esa.int/esasky/) in particular in UV, optical or X-ray. The ultraviolet allows to understand if they could be

confusion between various sources and the visible to see if the shape of the galaxy is visible. If the galaxy candidate has no bulge, seems to be irregular in optical and has no hard X-ray data but only soft X-ray, it is unlikely that the flux variation observed is due to an AGN. This page allows also to quickly consult the information regarding this coordinate on SIMBAD (https://simbad.u-strasbg.fr/simbad/ by right clicking on the candidate source. This website from CDS (Strasbourg astronomical Data Center) allows to check if the source is a known AGN or another particular object that could justify an ultraviolet flux variation. For the same purpose, the source is searched by its coordinates within the Swift sources catalog (https://www.swift.ac.uk/swift_live/index.php) to check if any label is associated to it, for example if it corresponds to a known GRB or a Supernova.

Fourthly, the coordinates are searched within the Dark Energy Spectroscopic Instrument (DESI) website (https://www.legacysurvey.org/viewer/desi-spectrum/dr1/) to search for its spectrum. If a spectrum is available the amplitude of the $[NII]\lambda_{6853}$ peak with respect to $H_\alpha\lambda_{6563}$ peak is observed as well as the amplitude of the $[OIII]\lambda_{5007}$ peak with respect to $H_\beta\lambda_{4861}$ peak to determine if the object is on the passive or the active side of the Baldwin, Phillips & Terlevich (BPT) diagram presented on figure 15. The passive sources are on the left area of the diagram and the active ones on the right.

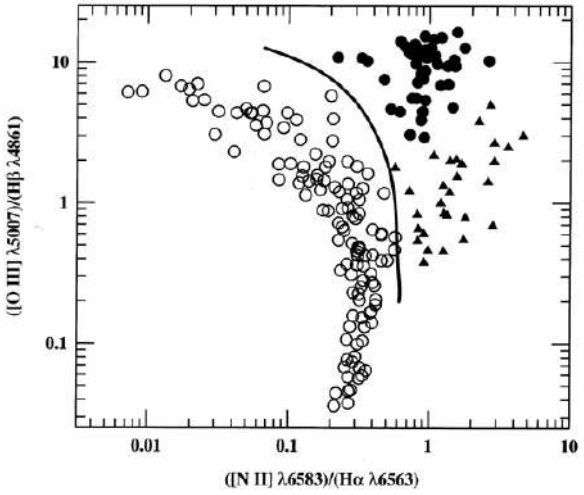

Figure 15: BPT diagram from Veilleux and Osterbrock, 1987

3 Results

Applying the methods presented previously, 27 objects have been retained. From those:

- 10 are retained as TDE candidates.
- 5 are interesting identified variable UV objects but not TDE (2 AGN, 1 GRB, 2 supernovas)
- 10 are interesting not identified variable UV objects unlikely TDE.
- 2 are not confirmed data (one suspicious match and one GALEX detection date that cannot be confirmed).

As filters applied aims to find TDE, the found objects type repartition is not representative of the repartition over the whole combined UV catalog.

3.1 Presentation of the best TDE candidates

In the table 1 are presented the 10 TDE candidates characteristics. The supposed black hole mass $M_\bullet$ in the center of these galaxies is deduced using the Regalade galaxy mass estimation M_{gal} and the Mummery et al., 2024 empirical formula for intermediate-mass black hole :

$$\log_{10}(M_\bullet/M_\odot) = \alpha + \beta \log_{10}(\frac{M_{gal}}{3 \times 10^{10} M_\odot}) \tag{7}$$

Where $\alpha = 7.44 \pm 0.04$ and $\beta = 1.42 \pm 0.07$ Note that as this relationship is linear, the lower the mass of the black hole, the lower is also the mass of the galaxy. The candidates have all, indeed, a mass between 9 and 11 $\log(M_\odot)$ which corresponds to small to mid-range galaxies. Having such UV variations in nuclei of such small galaxies enhances the probability that the observed variations are TDE-related and not AGN-related. Additionally, the absolute plateau luminosity L has been estimated using the final recommended distance provided by the Regalade catalog (d in parsec converted to cm) and the supposed plateau flux observed in UVW2 (F in erg s^{-1} cm^2 A^{-1}) for each candidate according to the classical formula :

$$L = 4\pi d^2 \times \Delta\lambda \times F \tag{8}$$

Where $\Delta\lambda$ is the effective band width in UVW2 of the corresponding instrument.

Source ID	RA (°)	DEC (°)	TDE date (MJD)	BH mass ($\log M_\odot$)	Plateau luminosity log_{10}(erg s^{-1})	Wise color (W1-W2 mag)	X-ray (Hard/Soft)	BTP diagnostic
44098	53.04583	-27.97073	54625 ± 175	7.0	42.1	0.47	No/Yes	-
45292	53.83036	-24.91328	53950 ± 150	7.6	42.9	0.03	No/No	-
124333	157.60286	45.16580	54550 ± 150	5.8	42.9	0.05	No/No	-
128873	162.28371	22.89408	53850 ± 50	-	42.7	0.50	No/No	-
190956	208.31370	5.10284	53820 ± 50	8.1	41.6	0.55	No/Yes	No line
208380	223.41889	3.42184	54050 ± 50	8.1	42.9	0.23	No/Yes	-
214117	228.37902	-9.01322	54500 ± 300	6.2	42.4	0.48	No/Yes	-
229525	250.36230	69.05079	54300 ± 100	8.1	42.6	0.47	No/No	-
230085	250.83309	39.93868	54200 ± 20	7.0	42.9	0.35	No/No	-
259263	329.73810	-30.04612	54230 ± 230	7.1	42.3	0.56	No/No	-

Table 1: Best candidates obtained characteristics

The figure 16 also presents the position of the candidates in the galactic coordinates. As expected, no candidate has been found near the direction of our galaxy center, where only a few galaxies are visible due to dust and gas extinction.

The indicated TDE date corresponds to the mean date of the two measurements between which the flux jump is observed.

The black hole masses correspond to low mass supermassive black holes reaching at maximum 10^8 $M_\odot$ which is consistent with the masses inferred from the sample of TDE used in Mummery et al., 2024. This is encouraging, as the maximum expected mass for a black hole that could disrupt a main sequence star is around 10^8 $M_\odot$ for a non-spinning black hole, or up to 7×10^8 $M_\odot$ for a maximally spinning black hole, as mentions Gezari (2021).

For all the candidates, W1-W2 mag is lower than 0.8 and no hard X-ray have been measured, two indices that tend to show that it is not AGN. Unfortunately, almost none of these objects have a DESI spectra available to identify if it is in the passive area and the only one with a spectra has no visible line to perform the diagnostic.

From the computation, all sources have a luminosity between $10^{41.5}$erg s^{-1} and 10^{43}erg s^{-1} that is consistent with the values proposed by Mummery et al., 2024. Using this paper, another criterion

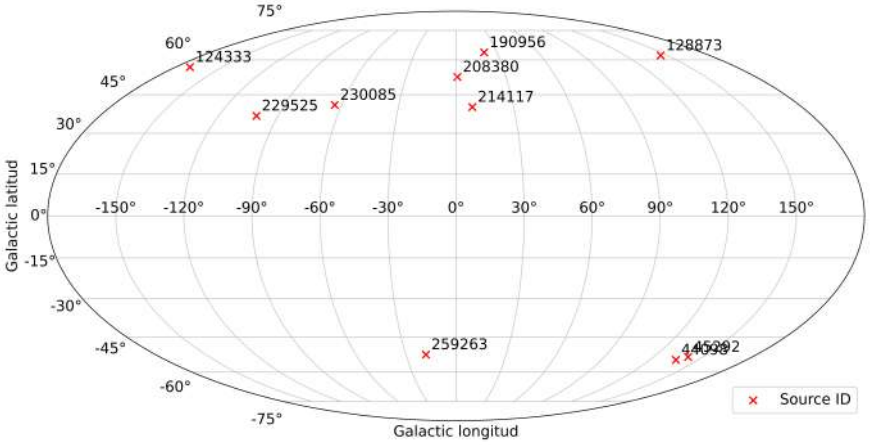

Figure 16: Candidates galactic positions

could be to check the scaling relationship between the black hole mass and the plateau luminosity. The figure 17 shows the position of the candidates in terms of plateau luminosity and inferred black hole mass with respect to the fit proposed by Mummery et al., 2024. Note that in this paper, no dispersion on this fit is proposed. It shows that candidates **124333** and **190956** seem outliers with respect to the fit. Note also that the errors computed in luminosity are optimistic as they are not considering any dispersion on the distances indicated in Regalade catalog. Looking in details the candidate **124333** light curves Figure 18, it shows a great variability in UVW2 (flux divided by 2 in a few days just before the supposed TDE) which could make doubt that the jump really corresponds to a TDE or that the measurement from Swift is correct. The candidate **190195** does not show such issue; the only doubt could be that the floor phase corresponds to UVOT data whereas the plateau phase corresponds to OM data, even if the optical flux matches one to another.

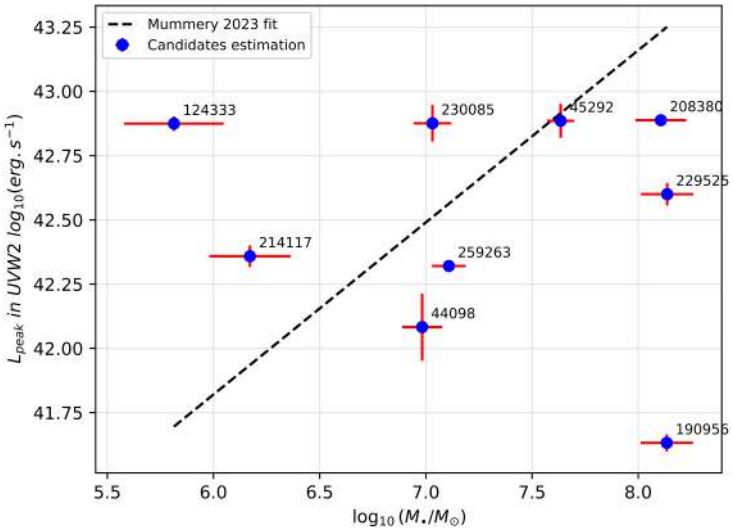

Figure 17: Relationship between black hole mass and plateau luminosity

Also the candidate **230085** shows a flux variability from one to double during the supposed plateau phase. It is hard to distinguish if it corresponds to a real variability or if the UVOT errors associated to the flux are underestimated.

In general, the candidates light curves are not visually striking, but it fulfills the expected to

be considered as possible TDE. Most of it does not require to combine catalogs information (most are UVOT data related candidates), which gives confidence that no calibration issues could lead to detect a flux jump. The one requiring various catalogs to confirm a jump in UVW2 in particular (candidates **44098**, **229525**, **259263**) would need to go back to the raw data to ensure of the photometry computation alignment.

The light curves are shown including optical band information available in the catalog, as it could add interesting tendency. In general, the jumps corresponding to the plateau are associated with a flat activity in optical, which is expected in the cases of TDE, as only the initial flare is visible in optical which lasts a short period (around weeks). Actually, for candidate **128873** a peak in V band is visible before the supposed UV plateau (at the same date UVM2 is still on its floor value), which could correspond to the initial flare.

Note that the candidate **208380** shows only the jump in UVW2 and not UVM2 which remain constant. As no such details have been observed until now on confirmed TDE, it is not possible to ensure this is a coherent behavior. We could expect the TDE to affect the most energetic bands and possibly not UVW1 which is less energetic. But if this candidate is confirmed, it would be the first time we observed a TDE that affected only UVW2 and not UVM2.

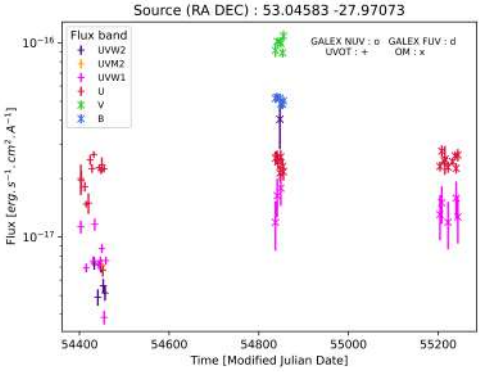

(a) Source 44098

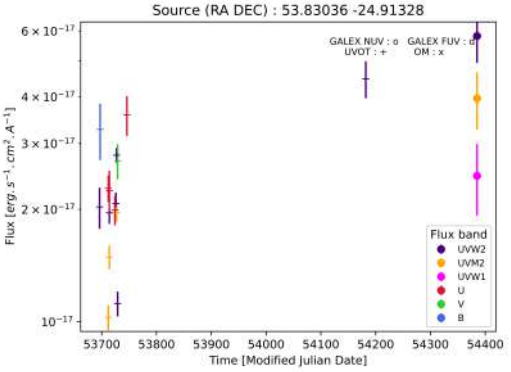

(b) Source 45292

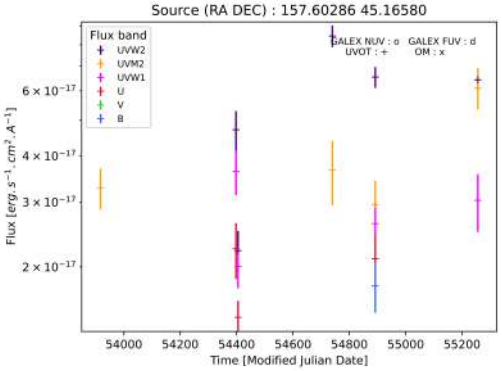

(c) Source 124333

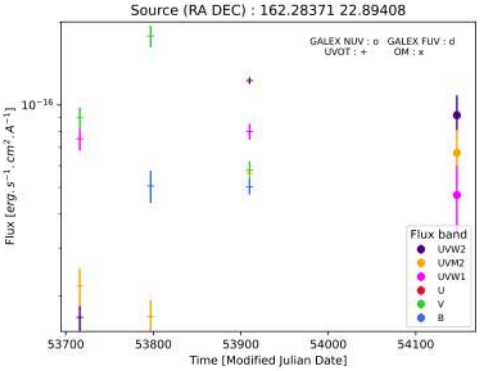

(d) Source 128873

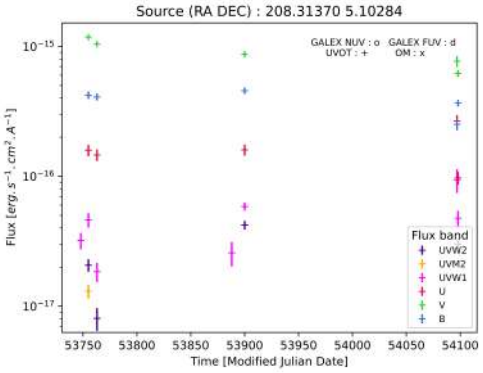

(e) Source 190956

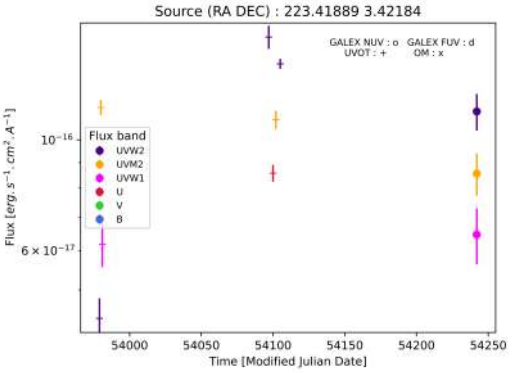

(f) Source 208380

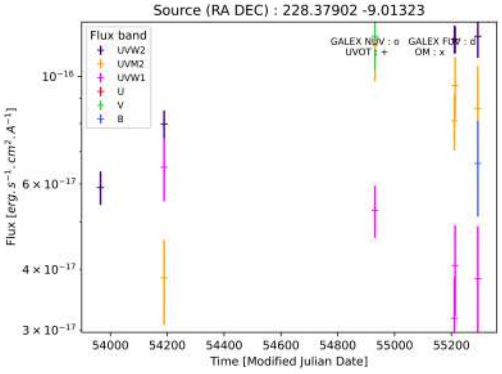

(g) Source 214117

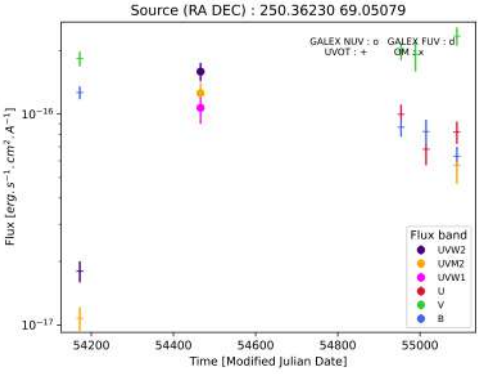

(h) Source 229525

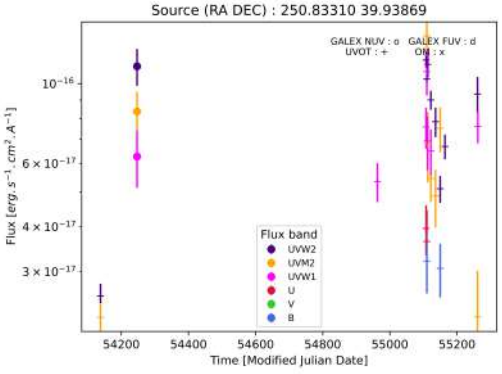

(i) Source 230085

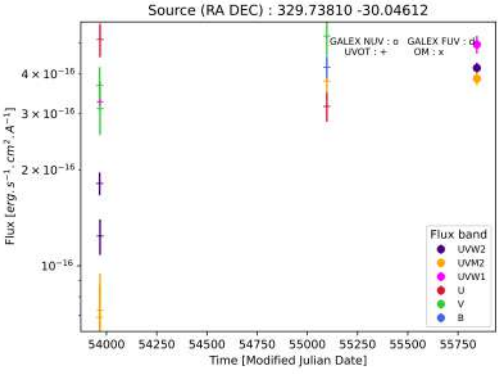

(j) Source 259263

Figure 18: Candidates light curves in all bands available in the catalog

3.2 Presentation of some other variable UV objects obtained

Some objects obtained during the scanning of the data presented a jump but could have been recognized as not being a TDE when analyzing the source information. Two of it are mentioned here, the supernova **SN 2008am** and the **GRB 061126** which light curves are presented in Figure 19.

It is possible to appreciate the peak of luminosity of the supernova (flux multiplied by almost 10 in UVW1) in 2008 and quickly decreasing back. For the GRB object, the light curve shows quick UV variation (flux multiplied by around 3 in 10 days and going back down), corresponding to the

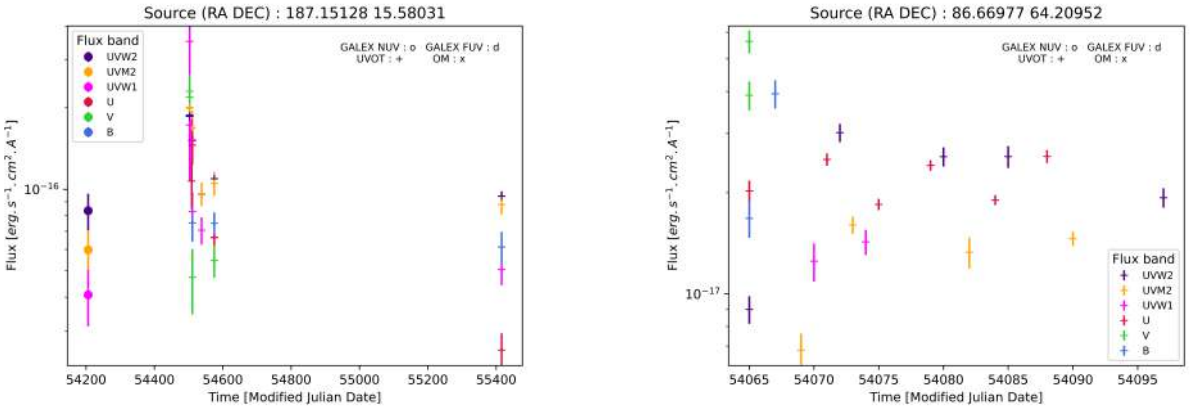

(a) Supernovae SN 2008am

(b) GRB 061126

Figure 19: Others object light curves

GRB afterglow. These examples that have been found casually when searching for TDE pattern recall the potential of the combined UV catalog that contains more than TDE signatures.

4 Discussion

After analyzing 22 years of UV bands data including 564,341 different galaxies, we obtained 10 consolidated TDE candidates. The expected theoretical TDE rate is not well defined and the best estimations are around 1×10^{-4} year^{-1} galaxy^{-1} (Gezari, 2021). Applied to our data, considering the TDE rate as constant over our time frame, this would correspond to around 1,250 events that would have occurred on our sample of galaxies in 22 years, as a rough estimation. Considering the density of data required to detect the shape of the UV plateau, we can expect our consolidated candidate number to be much lower. In particular, it is necessary to have points before the event, at UV floor, and after the event at UV plateau to be able to identify a TDE UV signature. Looking at the list of 187 known TDE with events reputed to be in our data time frame (from 239 in total in OTTER), we get, indeed, only 3 TDE with a significant shape in our data, which corresponds to 1.6%. The same ratio applied to 1250 galaxies gives a rough evaluation of 20 TDE expected to be visible in the data.

The "missing" TDE with respect to the expected could be due to limitations in the methods used. For example, the choice to filter the TDE with a flux jump only in the most energetic band (UVW2 and UWM2) and not in UVW1 band could limit the number of detected TDE. Otherwise, the simplicity of the filters applied would have led to get thousands of potential candidates to visually inspect which would not be manageable in the frame of this work. A solution would have been to use more complex filters, for example applying a machine learning algorithm, using models of TDE for the training based on the shape of the known TDE.

In any case, we see that the quality of our data (e.g. number of points in time series available, precision of the instruments, precision of the calibration) limits the number of TDE detectable. In particular, the number of points in time series available is scarce. For example, from the 564,341 galaxies in the catalog, 148,799 are purely optical and therefore cannot be used to find UV plateau. From the resting objects only 59,911 have more than two UV measurements, whatever the UV band, that is 10.6% of the initial galaxy sources number. Also the UVOT catalog which contains around half of the sources encompasses only 5 years and not the total 22 years, which reduces the probability to observe a TDE in its dataset.

In general, at this point to consolidate our candidates, it would be necessary to turn back to the raw data instead of the processed catalog data, in order to align the astrometry methods, in particular for extended sources, and better estimates background. In addition, the consolidated candidates will need a monitoring to confirm the UV plateau shape. This could be a future observation proposal for Swift cycle 23, as projects for cycle 22 have already been shortlisted (https://swift.gsfc.nasa.gov/proposals/c22_acceptarg.html). Otherwise, it could also be a proposal for ULTRASAT (Ultraviolet Transient Astronomy Satellite) that will be launched in 2027 and will precisely detect and monitor transient astronomical events in the near ultraviolet (https://www.weizmann.ac.il/ultrasat/).

Conclusion

In this work, we performed two main tasks:

- We created a combined UV catalog with UVOT, OM and GALEX data, matching the sources and calibrating the flux. Only galaxies matching with Regalade have been maintained in this version of the catalog for a total of 564,341 sources.
- We filtered the best TDE candidates, obtaining 10 consolidated candidates according to various criteria (UV light curve shape, multi-wavelength information, mass). We also identified 2 supernovas, 1 GRB, 2 AGN and stored 10 curious unidentified UV objects.

This last task is promising for TDE detection and, more generally, interesting UV objects selection within past UV data. However, the quality of the data is limiting and a deep dive within the instruments raw data would be necessary before trying any more complex approach (e.g. machine learning on synthetic TDE models) to confirm our candidates. Another approach to confirm their nature, would be to monitor them with current or future satellites, Swift or ULTRASAT for instance. If confirmed, our work will feed with additional information the existing TDE emission models, as it provides light curves according to various bands in UV (UVW2, UVM2 and UVW1).

Bibliography

Bentley, J. L. (1975). Multidimensional binary search trees used for associative searching. *Commun. ACM*, *18*(9), 509–517. https://doi.org/10.1145/361002.361007

Bianchi, L., Shiao, Bernie, & David, T. (2017). Revised catalog of galex ultraviolet sources. i. the all-sky survey: Guvcat_ais. *The Astrophys. Journal Supplement Series*, *230*(2), 24. https://doi.org/10.3847/1538-4365/aa7053

Gezari, S. (2021). Tidal disruption events. *Annu. Rev. Astron. Astrophys*, *59*, 21–58. https://doi.org/10.1146/annurev-astro-111720-030029

Mummery, A., van Velzen, S., Nathan, E., Ingram, A., Hammerstein, E., Fraser-Taliente, L., & Balbus, S. (2024). Fundamental scaling relationships revealed in the optical light curves of tidal disruption events. *Monthly Notices of the Royal Astronomical Society*, *527*(2), 2452–2489. https://doi.org/10.1093/mnras/stad3001

Page, M. J., Brindle, C., Talavera, A., Still, M., Rosen, S. R., Yershov, V. N., Ziaeepour, H., Mason, K. O., Cropper, M. S., Breeveld, A. A., Loiseau, N., Mignani, R., Smith, A., & Murdin, P. (2012). The xmm-newton serendipitous ultraviolet source survey catalogue. *Monthly Notices of the Royal Astronomical Society*, *426*(2), 903–926. https://doi.org/10.1111/j.1365-2966.2012.21706.x

Page, M. J., Yershov, V. N., Breeveld, A. A., Mignani, R., Smith, P. J., Rawlings, J. I., Oates, S. R., Siegel, M., & Roming, P. W. A. (2015). The swift uvot serendipitous source catalogue. *Proceedings of Science*, (37). https://doi.org/10.48550/arXiv.1503.06597

Rees, M. J. (1988). Tidal disruption of stars by black holes of 106–108 solar masses in nearby galaxies. *Nature*, *333*, 523–528. https://doi.org/10.1038/333523a0

Stern, D., Assef, R. J., Benford, D. J., Blain, A., Cutri, R., Dey, A., Eisenhardt, P., Griffith, R. L., Jarrett, T. H., Lake, S., Masci, F., Petty, S., Stanford, S. A., Tsai, C.-W., Wright, E. L., Yan, L., Harrison, F., & Madsen, K. (2012). Mid-infrared selection of active galactic nuclei with the wide-field infrared survey explorer. i. characterizing wise-selected active galactic nuclei in cosmos. *The Astrophysical Journal*, *753*(1), 30. https://doi.org/10.1088/0004-637X/753/1/30

Tranin, H., Blagorodnova, N., Gómez-Muñoz, M., Wavasseur, M., Groot, P. J., Landsberg, L., Stoppa, F., Bloemen, S., Vreeswijk, P. M., Pieterse, D. L. A., van Roestel, J., Scaringi, S., & Faris, S. (2026). A catalog to unite them all: Regalade, a revised galaxy compilation for the advanced detector era. *Astronomy and Astrophysics*, *706*(A284). https://doi.org/10.1051/0004-6361/202556896

van Velzen, S. (2019). Late-time uv observations of tidal disruption flares reveal unobscured, compact accretion disks. *The Astrophys. Journal*, *878*(82,83). https://doi.org/10.3847/1538-4357/ab1844

Veilleux, S., & Osterbrock, D. E. (1987). Spectral Classification of Emission-Line Galaxies. *Astrophysical Journal Supplement*, *63*, 295. https://doi.org/10.1086/191166

Winter-Granic, M., & Quataert, E. (2025). Viscously spreading accretion disks around black holes: Implications for tdes, lfbots and other transients. *Journal of Astrophysics*. https://doi.org/10.48550/arXiv.2512.09017

Appendix A Additional figures

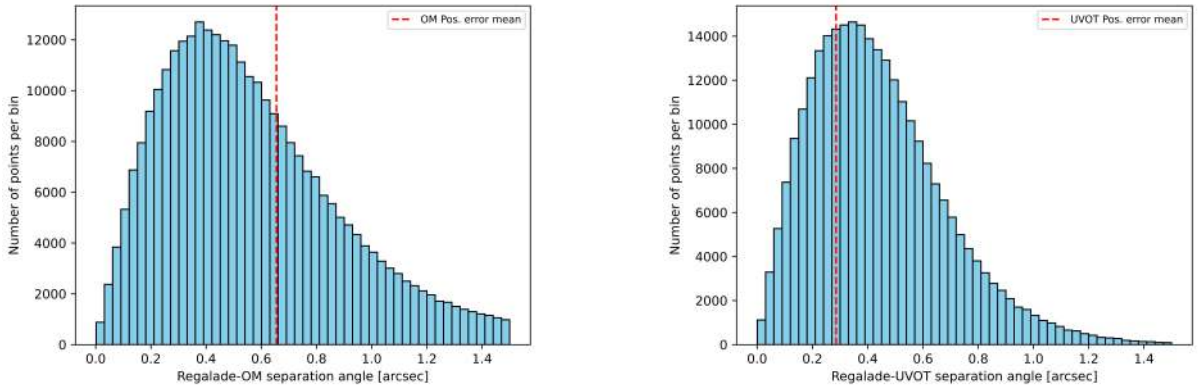

(a) OM-Regalade

(b) UVOT-Regalade

Figure A.1: Matching sources angular distance distribution

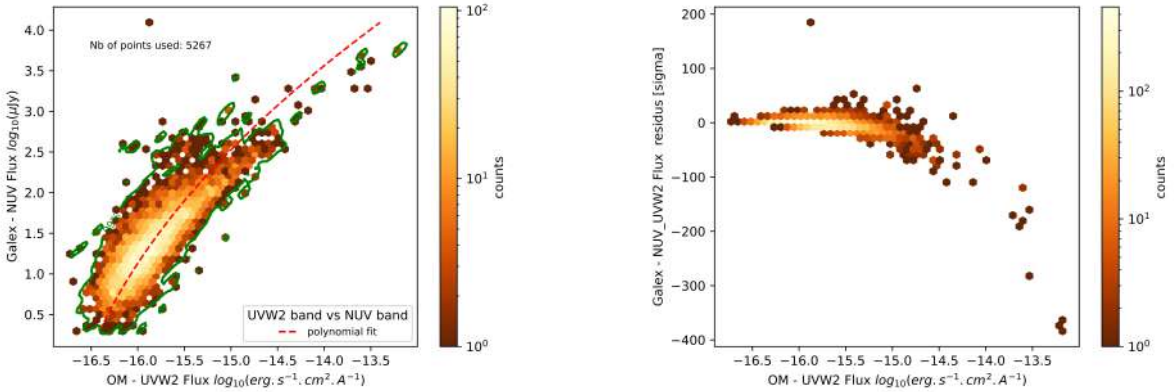

(a) GALEX vs OM flux per source

(b) GALEX residuals versus OM flux

Figure A.2: GALEX calibration with respect to OM for UVW2 band

Appendix B Calibration results

Instruments and bands	X^0	X^1	X^2	X^3
UVOT vs OM UVW2 (extended)	-4.706	0.517	-0.012	0.000
UVOT vs OM UVM2 (extended)	-0.419	0.760	-0.013	0.000
UVOT vs OM UVW1 (extended)	-0.377	0.730	-0.016	0.000
UVOT vs OM U (extended)	-0.378	0.738	-0.015	0.000
UVOT vs OM B (extended)	-0.140	0.758	-0.015	0.000
UVOT vs OM V (extended)	-7.183	0.214	0.000	0.001
UVOT vs OM UVW2 (not extended)	-5.325	0.484	-0.011	0.000
UVOT vs OM UVM2 (not extended)	-5.376	0.483	-0.011	0.000
UVOT vs OM UVW1 (not extended)	-4.327	0.533	-0.013	0.000
UVOT vs OM U (not extended)	-4.617	0.521	-0.012	0.000
UVOT vs OM B (not extended)	-3.321	0.582	-0.014	0.000
UVOT vs OM V (not extended)	-2.725	0.610	-0.014	0.000
GALEX NUV vs OM UVW2	-16.515	0.340	0.103	0.000
GALEX NUV vs OM UVM2	-16.716	0.374	0.126	0.000
GALEX NUV vs OM UVW1	-16.957	0.363	0.213	0.000
GALEX FUV vs OM UVW2	-16.212	0.135	0.180	0.000
GALEX FUV vs OM UVM2	-16.535	0.265	0.176	0.000
GALEX FUV vs OM UVW1	-16.860	0.437	0.180	0.000

Table B.1: Calibration coefficients for each instrument and each band